JOURNAL OF AIRCRAFT
Vol. 44, No. 2, March–April 2007

Piezoelectric Transducer Actuated Leading Edge De-Icing with Simultaneous Shear and Impulse Forces

Suresh V. Venna,* Yueh-Jaw Lin,† and Galdemir Botura‡
University of Akron, Akron, Ohio 44325-3903

DOI: 10.2514/1.23996

Piezoelectric actuations for simultaneous generation of shear and impulse forces for effective and energy efficient de-icing applications are proposed in this paper. Aircraft leading edge structures are considered for analysis and lab experiments. Piezoelectric actuators are affixed on the inner surface of the leading edge at the locations where highest amount of ice accretion on the outer surface has occurred. Simultaneous shear and impulse force generation is achieved with actuators consisting of two sets of electrodes, one arranged in parallel to the poling direction, and the other perpendicular to it, to generate shear forces and normal forces, respectively. Finite element models of the leading edge structure with ice accretion layer are formulated. Simulations of the de-icing process are performed and the actuator locations, electric charge applied, and impulse duration are optimized to achieve effective ice removal. Experimental results reveal that the proposed de-icing method is clearly advantageous in that it employs a single actuator for both shear and impulse generation for de-icing, making it consume far less power than any existing aircraft de-icing methods (estimated 100 vs 2000 W) which leads to considerable weight reductions in the de-icing associated systems (estimated 20 vs 300 kg) on aircraft.

I. Introduction

A degradation of aircraft performance and safety due to ice accretions on aircraft structures is a major concern in the aircraft industry. Ice accretions on wings, tails, and engine components have severe effects on lift, control, and safety, to name a few. Aircraft leading edge is one of the structures most prone to ice accretions and several research works are focused on simulating the ice accretions and understanding the effects. Lynch and Khodadoust [1] published a comprehensive review of various experiments and results conducted to understand the effects of ice accretions on aircraft wing aerodynamics. Different types of ice accretions and their effects are reported. Experimental and computational simulation of in-flight icing phenomena was discussed by Kind et al. [2] and Venna and Lin [3]. Bragg et al. [4–8] conducted some research to predict, simulate, and understand the effects of ice accretions. Software codes such as LEWICE, developed by NASA, allow the simulations of ice accretions on aircraft components.

A number of de-icing methods are developed for removal of ice from aircraft wing structures. De-icing methods can be broadly classified as Kground de-icing and in-flight de-icing. Ground de-icing is done when the flight is at rest by spraying glycol based chemicals, etc., for removal of ice. However, in-flight antiicing is used to prevent ice accumulations when the flight is in air. Thermal in-flight antiicing methods prevent accumulation of ice by keeping the surfaces at elevated temperatures. These methods consume a very large amount of power. Electrical de-icing methods such as the electroimpulsive separation system (EESS), electromagnetic impulse de-icer (EIDI) and eddy current repulsion de-icing boot (ECRDIB) are discussed by Reinmann et al. [9]. pneumatic impulse ice protection system (PIIP) [10] employs a stretchable fabric-reinforced elastomer boot, which is supplied with impulse of high-pressure air to expand the boot, resulting in removal of ice. Use of thin shape memory alloy (SMA) sheet to achieve de-icing is proposed by Ingram et al. [11]. Ramanathan et al. [12] developed a technique for de-icing of helicopter blades by launching shear horizontal waves on the surface to be de-iced. Venna and Lin [13–15] proposed exciting the structure to natural frequencies to achieve de-icing. Electrical methods consume significant amount of power and can be too heavy.

There is always a strong demand for de-icing techniques that are effective and at the same time, lightweight, low in power consumption, low maintenance and manufacturing costs, reliable operation, and offer little or no design change requirement and aeropenalties. In this paper, such a de-icing method is proposed using piezoelectric actuators. The proposed de-icing technique is based on the fact that the adhesive bond of ice-substrate interface is relatively weak in shear. Piezoelectric actuators are used to produce local shears at the locations of ice accretion to weaken the interface and subsequently deice the surface with normal impulse forces. Elaborations on the adhesive strength of ice-substrate interface and piezoelectric properties are given in Secs. II and III, respectively. Development of a de-icing technique using finite element modeling and analysis is described and discussed in Sec. IV. Section V presents de-icing simulations and results. This is followed by experimental testing and implementation of the proposed de-icing concept in Sec. VI. Finally, Sec. VII concludes the paper.

II. Adhesive Strengths of Ice

To develop an effective de-icing technique, understanding of the adhesive strength of ice is critical. In this section, an overview of previous research focused on understanding the adhesive strengths of ice is provided. Raraty and Tabor [16] conducted several experiments to determine the interfacial strength of ice substrate. Jellinek [17] discovered that adhesive shear strength of ice-substrate interface is significantly lower than the adhesive tensile strength. Scavuzzo et al. [18,19] investigated the shear strength of rime and glaze ice. Ice adhesion to hydrophilic and hydrophobic surfaces was investigated by Bascom et al. [20]. Archer and Gupta [21] studied ice adhesion to Al 6061 alloy. Extensive literature review was provided by Ramanathan et al. in the bonding strengths of the ice-substrate interface [12]. The summary of the adhesive shear strengths of refrigerated and wind-tunnel ice, obtained from our literature survey, is given in Tables 1 and 2, respectively.

Based on the above values, it can be concluded that the maximum adhesive strength of refrigerated ice is around 1.7 MPa and that of

Received 17 March 2006; revision received 23 May 2006; accepted for publication 29 May 2006.

*Research Student, Department of Mechanical Engineering.
†Associate Professor, Department of Mechanical Engineering.
‡Research Student, Department of Mechanical Engineering; currently R&D Section Manager, Goodrich Corporation, De-icing and Specialty Systems, Uniontown, Ohio 44685.

Table 1 **Adhesive shear strengths of refrigerated ice**

Author	Substrate	Shear strength (MPa)
Loughborough	Al	1.52
Hass	Cu	0.85
Raraty and Tabor	Stainless steel (SS)	1.66
Bascom et al.	Polished SS	1.63
Ford and Nichols	Polished SS	0.24

Table 2 **Adhesive shear strength of wind-tunnel ice**

Author	Substrate	Shear strength (MPa)
Stallbrass and Price	Al	0.026–0.127
Chu and Scavuzzo	Al	0.2–1.03

wind-tunnel ice is around 1 MPa, whereas the tensile strength is around 274 MPa [21]. The ice crystal formation of refrigerated ice is considered to be glazed ice. This type of ice usually is smooth and hard to remove. Ice formed in the wind tunnel is largely rime ice, with a mix of some glaze ice. Because the ice crystal of this type is rough, it is easy to remove [22]. The strength values in Tables 1 and 2 are for temperature around $-5°C$. However, there are some arguments saying that wind-tunnel ice is stronger than the refrigerated ice. In the proposed technique, this weak shear bond of the ice-substrate interface is targeted.

III. Piezoelectric Properties and Actuation

Piezoelectric materials produce electric charge when strained and produce strains when an electrical charge is applied. The former property is called direct piezoelectric effect and the later, converse piezoelectric effect. This property makes the piezoelectric materials capable of coupling mechanical and electrical systems. The efficiency of this transformation is defined by the so-called piezoelectric electromechanical coupling coefficient (Table 3).

The electromechanical coupling coefficient in case of direct piezoelectric effect is defined as the square root of the electrical energy produced in the piezoelectric material to the mechanical energy supplied to it. In piezoelectric ceramics there are three modes of coupling that are of special importance. This may be understood through consideration of where one may apply the electrodes to the piezoelectric. The electrodes may be put in such a way that they are perpendicular to the electrical polarization, as shown in Fig. 1, called 3-location arrangement.

If voltage is applied to electrodes with electrodes placed at 3-location, the piezoelectric material changes both its longitudinal and lateral dimensions. If one couples, mechanically to the expansion in longitudinal direction, one measures k_{33}. If one couples to one of the lateral directions, one measures k_{31}, which is lower than k_{33}. Note that the reverse process corresponds to the same coupling values. By straining the material in the longitudinal direction, the electrical field is produced in direction 3, governed by k_{33}. Similarly, by straining the material in the lateral directions, the electrical field produced in 3-direction is governed by k_{31}. In both cases above, they are 3-location electrodes.

Table 3 **Properties of piezoelectric actuators**

Elastic properties: E_{11}	6.061E10 N/m^2
E_{22}	4.800E10 N/m^2
E_{33}	6.061E10 N/m^2
υ_{12}	0.512
υ_{13}	0.3
υ_{23}	0.512
G_{12}	25.64E07 N/m^2
G_{13}	23.67E07 N/m^2
Density:	7500 Kg/m^3
Dielectric properties: D_{11}	5.87E − 09 C/V m
D_{22}	4.83E − 09 C/V m
D_{33}	5.87E − 09 C/V m
Piezoelectric constants: $d_{ij}=$	3.22E − 03 m/V

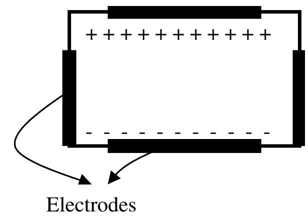

Fig. 1 **Placing of electrodes.**

IV. Finite Element Model and Analysis

Aluminum leading edge structure conforming to airfoil type NACA 001 is used. The length of the leading edge is 0.1524 m (6 in.). The two straight edges of the leading edge are fixed to the so-called "afterbody" (main portion of the wing). To exactly simulate the actual boundary conditions, the nodes close to the straight edges are given zero degrees of freedom. The prototyped leading edge structure that we refer to is shown in Fig. 2.

The leading edge structure shown above is affixed to two wood frames on the two vertical side edges, simulating the leading edge structure connected to the afterbody of an aircraft wing section in a real case. The boundary conditions may be changed depending on

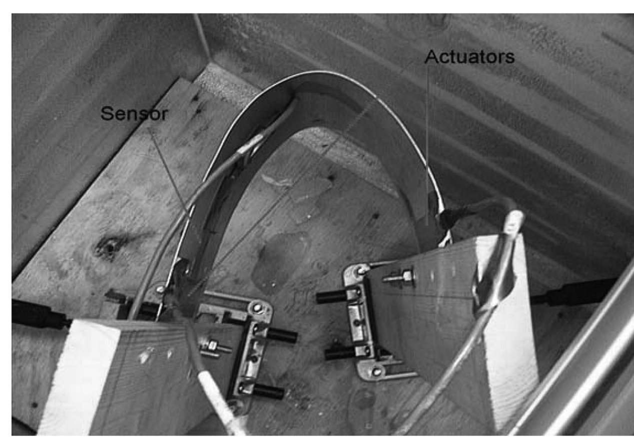

Fig. 2 **Physical prototype of the aluminum leading edge structure.**

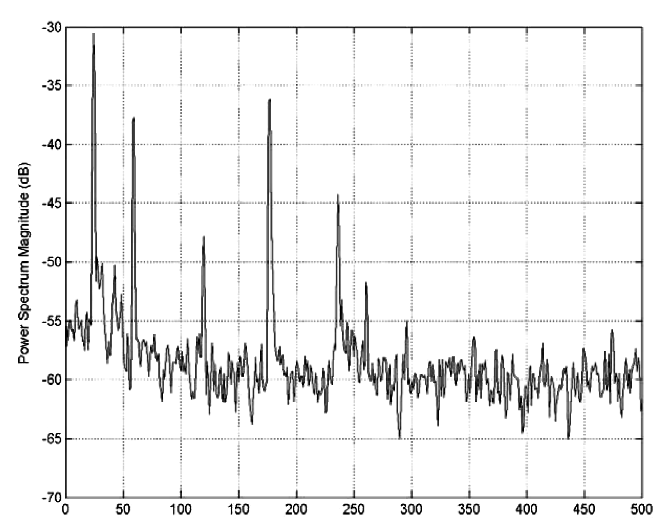

Fig. 3 **Frequency (in Hz) response of the leading edge.**

Table 4 A comparison of real and FEA-based natural frequencies of the aluminum leading edge structure

Mode #	Finite element model	Experiment
1	32.3	31.8
2	65.4	52.7
3	100.3	111.9
4	135.6	155.0
5	176.3	177.4

the clamped locations, tightness, etc. In our case, they were tight up with screws and nuts. Loosed attachments of the boundary conditions may lead to undesirable vibration due to piezoelectric transducer (PZT) activation for de-icing. The frequency responses of the prototyped aluminum leading edge structure are obtained experimentally and the collected data depicted in Fig. 3 below.

To ensure the accuracy and reliability of the follow-up finite element analysis (FEA)-based analysis and simulation, a comparison of the finite element and experimental values of the natural frequencies is made before further investigations using finite element models are conducted. The results of our comparison are summarized in Table 4.

From the above comparison, close agreement of the first five modes of natural frequencies between the real prototype and finite element model of the underlying airfoil leading edge structure is evidenced. This implies that our current approach of using finite element model for predicting the de-icing behaviors of various proposed actuating schemes on the prototyped leading edge structure is feasible.

Finite element models for the proposed configuration and analysis results are discussed in detail in the next section. ABAQUS is used for the finite element analysis and simulation in the entire investigation.

A. Finite Element Modeling

Finite element models of the leading edge, piezoelectric actuators and ice layer are constructed for different configurations. The type of elements used, boundary conditions, loads, and contact modeling are as follows:

1) Aluminum leading edge: 8-node three-dimensional continuum elements (C3D8),

2) Piezoelectric elements: 8-node three-dimensional piezoelectric elements (C3D8E),

3) Ice layer: 8-node three-dimensional continuum elements (C3D8).

Piezoelectric actuators are firmly attached to the inner surface of the leading edge. Appropriate surfaces of the leading edge elements and ice layer are defined and the contact between these surfaces is modeled as spot weld connections using the FASTENER option, which allows us to investigate the forces at these bonding locations. However, physical debonding of the ice layer is not shown in this analysis. ABAQUS/explicit has the debonding analysis capability, but it does not support piezoelectric elements and piezoelectric analysis. Because the objective of the work is to test the effectiveness of the proposed method and understand the interfacial stresses and forces, this kind of modeling and analysis will suffice.

Nodes close to the two flat edges of the leading edge, which would be attached to the afterbody, are given zero degrees of freedom (ENCASTRE). Sinusoidal loading of electric charge is applied to the piezoelectric actuators at different frequencies, which will be discussed in detail in the next several sections.

B. Finite Element Analysis

Steady state dynamic analysis (ABAQUS/standard procedure: STEADY STATE DYNAMICS) is performed to investigate the dynamic behavior of the structure. Sinusoidal loading of electric charge of five different magnitudes is applied to the piezoelectric actuators at 10 different frequencies. The five electric charge magnitudes are: $1\text{E}+01\ \text{Coulomb/m}^3$; $1\text{E}-01\ \text{Coulomb/m}^3$; $1\text{E}-03\ \text{Coulomb/m}^3$; $1\text{E}-05\ \text{Coulomb/m}^3$; $1\text{E}-07\ \text{Coulomb/m}^3$, and the ten frequencies of loading are 1, 5, 10, 20, 30, 50, 100, 500, 1000, and 1500 Hz.

The electric charge applied produces both shear and normal deformation of the piezoelectric actuators by virtue of the piezoelectric property d_{15}. Electrical charge is the only loading type allowed in this kind of procedure. For practical applications both the shear and normal deformations can be produced by applying voltage to the two sets of electrodes discussed earlier. Whether it is the charge or voltage applied it will not make any difference in the final results.

Field output requests are made for all the stress and strain components, displacements, velocities, and accelerations. History output of total kinetic energy and forces, moments, and total kinetic energy in the model are requested.

V. De-Icing Simulations and Results

De-icing simulations and results obtained for the following case of piezoelectric configuration are discussed in detail in this section. This proposed configuration uses two piezoelectric actuators ($34 \times 17 \times 7$ mm). The finite element model of the leading edge with the two piezoelectric actuators rigidly placed at the ends to the inner surface of the leading edge is shown in Fig. 4. Nine reference nodes along the interface are selected to investigate the forces in the bond, which are shown in Fig. 5.

Analysis is performed with all the electrical charge loads mentioned above. Loading of $1\text{E}-05\ \text{C/m}^3$ produced enough shear stresses and accelerations to achieve complete de-icing at 1000 Hz frequency. Loading with lesser charge did not produce enough shear stresses and de-icing. For loading values higher than

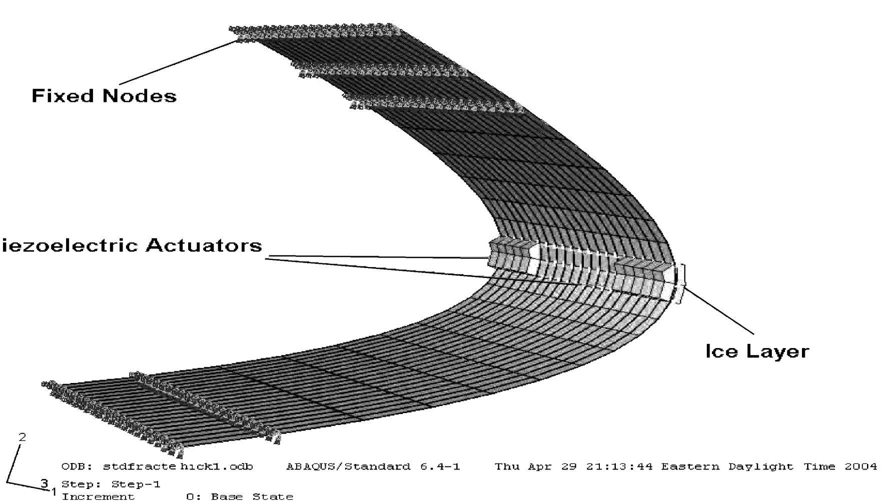

Fig. 4 Airfoil structure configuration with actuators and ice patches.

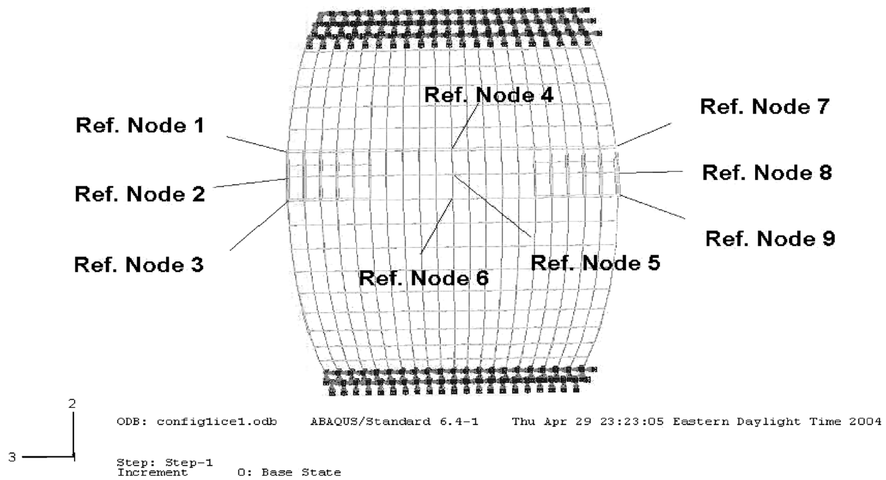

Fig. 5 The selected nine reference nodes in FEM.

1E − 05 C/m^3 , de-icing is achieved at other frequencies too. But, the energy spent may be unnecessary and hence, a charge value of 1E − 05 Coulomb/m^3 can be concluded to be the optimal value for this proposed configuration. The summary of stresses and accelerations are listed in Table 5. Variation of total bond force with frequency at the nine reference nodes is given in Fig. 6. The contour plots of the leading edge shear and normal stresses are given in Figs. 7 and 8, respectively.

Other alternative configurations of actuators (e.g., $40 \times 17 \times 7$ mm, or $135 \times 17 \times 7$ mm to cover the whole length) and their proposed placements (e.g., at the center of the leading edge, or covering the entire length) are also investigated using finite element simulations. After comparing the results, it is found that the first proposed configurations of PZT actuators and the placement yields the best performance.

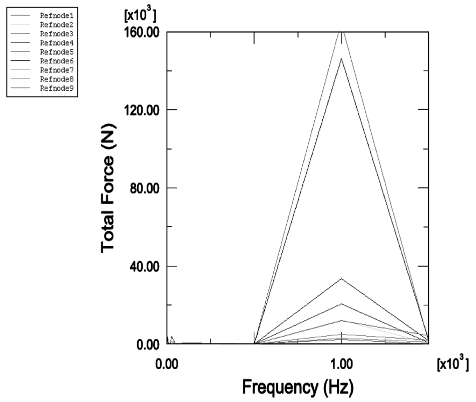

Fig. 6 Total force of the interface versus frequency.

VI. Experimental Testing and Implementation

Referring back to Fig. 2, a prototype model of the leading edge was made based on the specifications suggested by the industrial partners. Aircraft wing type NACA 0012 was assumed.

The thickness distribution for NACA four-digit wing sections [23] is given by

$$\pm y_t = \frac{t}{0.20}(0.2960\sqrt{x} - 0.12600x - 0.35160x^2 + 0.28430x^3 - 0.10150x^4)$$

where t is the maximum thickness expressed as the fraction of the chord. For the NACA 0012 section, the t is given by the last two digits (i.e, 12). The NACA 001 section is a symmetrical section. The two straight edges of the leading edge considered are fixed to the afterbody (main portion of the aircraft wing structure).

As mentioned in the previous section, it is proposed that two piezoelectric actuators are attached on the inside of the leading edge structure for removing the ice patches formed on the outside of the same configuration. In addition, a piezoelectric sensor is attached to the structure too, which enables the system to capture the symmetric modes very effectively. Figure 9 shows the lab de-icing test rig for the experimental implementation.

Actuators placed inside the curved leading edge area is connected to the arbitrary waveform generator through an amplifier. The arbitrary waveform generator generates the necessary signals to actuate the structure with control commands given by a build-in dSpace PC processor. The amplifier then amplifies the input signal to the actuator, so that a desired amount of deflections is generated to remove the ice patches. The sensor also placed inside the curved structure near the actuators is connected to an oscilloscope to visually examine the responses of the airfoil structure. In the real aircraft leading edge structure, only the width of the structure used in the experiments needs to be scaled up to reflect the reality. The length and thickness remain the same. Therefore, to obtain the anticipated

Table 5 Summary: Analytical data of the actuated leading edge with loading of 1E − 05 C/m^3

Frequency (Hz)	Max. shear stress (N/m^2)	Max. normal stress (N/m^2)	Rotational acceleration (Rad/s^2)	Normal acceleration (m/s^2)
1	5.28E + 05	2.49E + 06	9.02E − 01	7.51E − 02
5	2.44E + 06	1.05E + 07	1.04E + 02	8.86E + 00
10	6.56E + 04	3.01E + 05	8.38E + 00	7.23E − 01
20	1.60E + 05	3.65E + 05	9.39E + 01	7.50E + 00
30	3.24E + 05	1.28E + 06	3.51E + 02	3.40E + 01
50	4.43E + 05	1.13E + 06	1.67E + 03	1.47E + 02
100	2.84E + 05	8.24E + 05	1.25E + 02	2.65E + 02
500	2.78E + 05	6.78E + 05	2.12E + 03	5.36E + 02
1000	7.54E + 06	2.49E + 07	7.40E + 04	8.70E + 03
1500	6.44E + 05	1.80E + 06	1.45E + 04	1.25E + 03

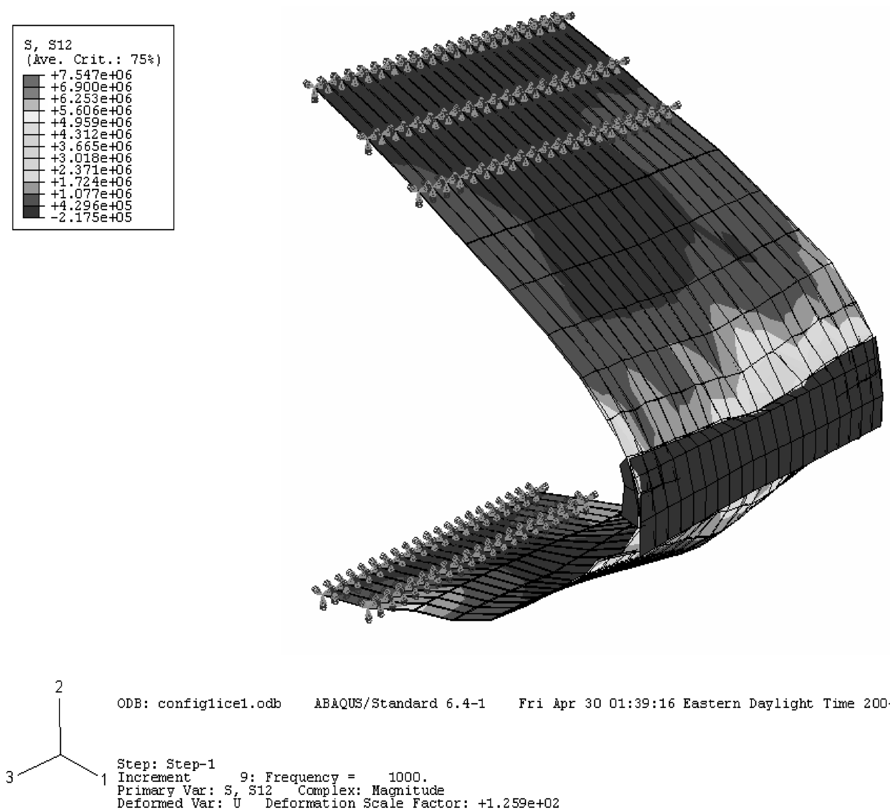

Fig. 7 Contour plot of shear stress at 1000 Hz frequency.

de-icing results, PZT can be scaled with that of the width of the leading edge structure.

Two ice patches are formed on the tip of the leading edge affixed on wood beams in a powerful commercial freezer as shown in Fig. 10. Ice patches are approximately of dimensions $3 \times 25 \times 50$ mm. These ice patches are firmed and adhered enough onto the substrate that they are difficult to be removed by hands.

To experimentally verify the concept proposed in this work and the FEA simulations presented in Sec. V, a number of trials of the de-icing tests were conducted at 10°F temperature in the freezer. The

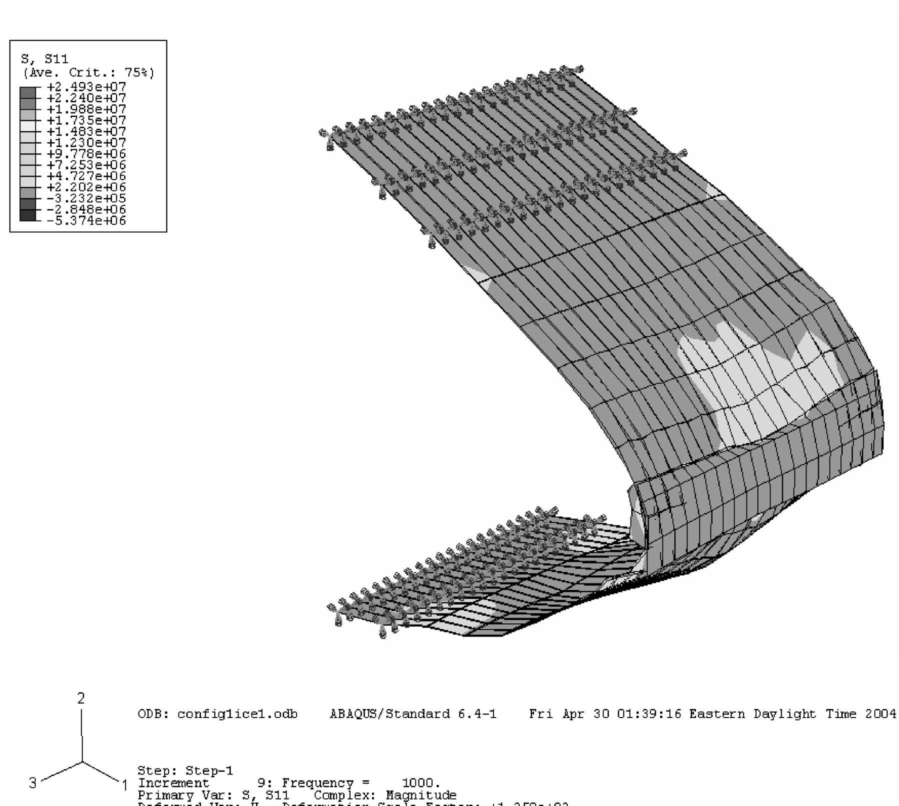

Fig. 8 Contour plot of normal stress at 1000 Hz frequency.

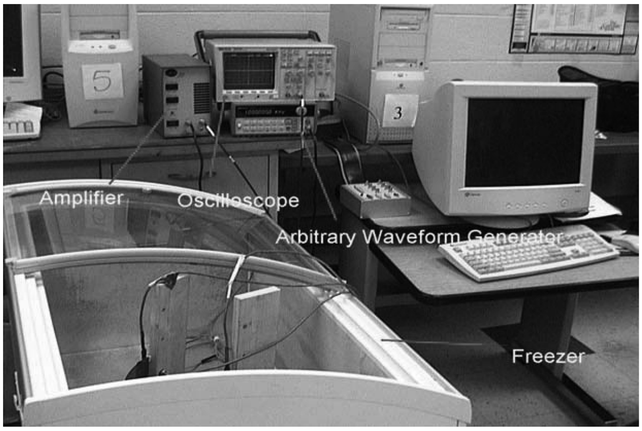

Fig. 9 Lab testing rig for de-icing conducted in a freezer with a temperature range of 5–25°F.

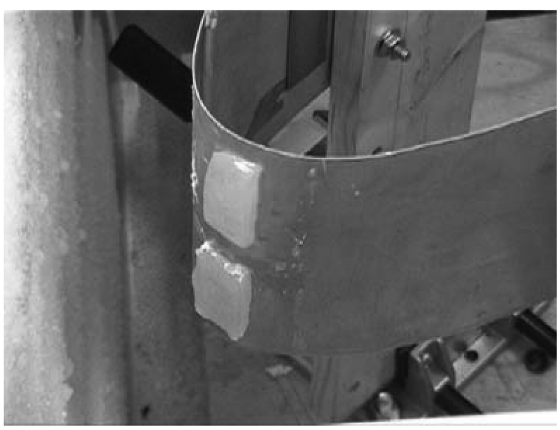

Fig. 10 Ice patches sticking firmly on the leading edge in a freezer.

Fig. 11 Snap shots of the de-icing (at 10°F) sequence after triggering the proposed method in 30, 80, and 127 s.

experimental results showing the process of ice patches detaching from the leading edge are given in Fig. 11. The recorded time of de-icing (counting from the beginning of the proposed simultaneous actuation) for the three snap shots in the figure are 35 , 80 , and 127 s, respectively. It can be seen that the ice patches were fully removed after 127 s of implementing the proposed de-icing method at this constant temperature. The de-icing experiments are also done at other temperatures including 5, 15, and 20°F. To consider generalized case of ice accretion, the prototype with a whole piece of ice patch (approximately of dimensions 3 mm × 25 mm× 200 mm) adhered on the leading edge (see Fig. 12) is also tested with the same set of temperatures kept in the commercial freezer.

It is found that the de-icing time obtained for the one larger ice patch is higher than that for the two ice patches on the leading edge. The de-icing time in seconds recorded for all five different temperatures and two types of ice patches are listed in Table 6.

Based on the testing results in terms of de-icing time, it reveals that approximately 10% longer time is required for removing the larger patch of ice than doing the two smaller patches at low temperatures. However, at higher temperatures (15 and 20°F) the de-icing time for both cases are about the same. The real in-flight icing involves airflow. In general, it reduces the adhesive strength of ice accreted on

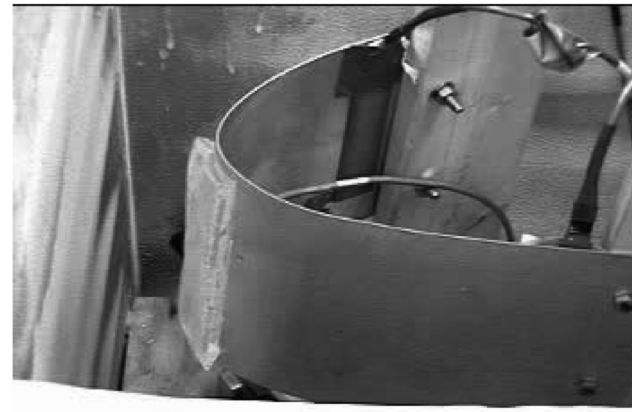

Fig. 12 One large ice patch (covering whole width) formed and adhered firmly on the leading edge in a freezer.

structure surface. Therefore, airflow usually shortens the de-icing time when compared with that of the lab experimental results. On the other hand, ice layer de-icing, by intuition, should be more difficult than ice patch de-icing. Comparing the experimental results of the current work with those of the authors' earlier work [14,15], it is found that the proposed simultaneous shear and impulse de-icing method performs more than 40% better (in shortening de-icing time) than employing shear forces for de-icing alone.

VII. Conclusion

A novel method for de-icing of leading edge structures was proposed. Weak shear bond between the ice and substrate is targeted to achieve de-icing. Local shear forces are generated by attaching a piezoelectric actuator on the inner surface of the leading edge where ice accumulation is the highest. Five different electric charge loads were applied to the piezoelectric actuators at ten different frequencies for a designated configuration of piezoelectric actuators. Optimal combination of frequency and critical charge were determined for the configuration from the analysis results. This configuration yielded a high amount of stresses and forces with a low amount of applied charges. The de-icing experiments were carried out in the lab tested at four temperatures, 5, 10, 15, and 20°F in a freezer. Two types of ice accretion scenarios were considered for the de-icing implementation. All cases were conducted successfully with adhered ice patches completely removed from the leading edge surface by the proposed de-icing method. The comparison of results indicated that a single ice patch was more difficult to remove than two separated smaller patches. It is also noted that the proposed simultaneous shear and impulse de-icing method performs more than 40% better (in shortening de-icing time) than employing only shear forces for de-icing. Moreover, this proposed method utilized over an order of magnitude less power (estimated 100 vs 2,000 W) than other existing de-icing methods, which is desirable for aircraft design. Effective utilization of the input energy is achieved by placing the actuators at the locations to be de-iced and targeting the weak shear bond. Although the lab experiments were conducted successfully, there are still many technical issues that need to be resolved if it were to go on a real aircraft. The proposed de-icing system was only tested on a simplified representation of a wing with a simplified representation of ice accretion.

Table 6 Summary of de-icing time in seconds at four different temperatures and for two ice types

Freezer temperature (°F)	Average de-icing time (sec) two ice patches	Average de-icing time (sec) one large ice patch
5	223	251
10	127	148
15	85	88
20	66	67

Acknowledgments

The first two authors gratefully acknowledge the sponsor and financial support to this work through an OAI CCRP grant and The Goodrich Corporation. Dave Sweet's suggestions and support during the course of this work were also appreciated.

References

[1] Lynch, F. T., and Khodadoust, A., "Effects of Ice Accretions on Aircraft Aerodynamcis," *Progress in Aerospace Sciences*, Vol. 37, No. 3, 2001, pp. 669–767.

[2] Kind, R. J., Potapczuk, M. G., Feo, A., Golia, C., and Shah, A. D., "Experimental and Computational Simulation of In-Flight Icing Phenomena," *Progress in Aerospace Sciences*, Vol. 34, No. 2, 1998, pp. 257–345.

[3] Venna, S., and Lin, Y. J., "PZT-Actuated In-Flight De-Icing with Simultaneous Shear and Impulse Forces," *Proceedings of International Mechanical Engineering Congress and Exposition 2004, Adaptive Materials and Systems Symposium*, Vol. ASM 2B, ASME Press, New York, NY, Nov. 2004, pp. 92–98.

[4] Broeren, A. P., and Bragg, M. B., "Effect of Airfoil Geometry on Performance with Simulated Intercycle Ice Accretions," *Proceedings of the 41st AIAA Aerospace Sciences Meetings & Exhibit*, AIAA Publishing, Reston, VA, Jan. 2003, pp. 212–218.

[5] Pan, J., Loth, E. , and Bragg, M., "RANS Sumulations of Airfoils with Ice Shapes," *Proceedings of the 41st AIAA Aerospace Sciences Meetings & Exhibit*, AIAA Publishing, Reston, VA, Jan. 2003, pp. 122–127.

[6] Lee, S., and Bragg, M. B., "Investigation of Factors Affecting Iced-Airfoil Aerodynamics," *Journal of Aircraft*, Vol. 40, No. 3, 2003, pp. 499–508.

[7] Gurbacki, H. M., and Bragg, M. B., "Unsteady Aerodynamics Measurement on an Iced Airfoil," *Proceedings of the 40th AIAA Aerospace Sciences Meetings & Exhibit*, AIAA Publishing, Reston, VA, Jan. 2002, pp. 151–159.

[8] Broeren, A. P., Addy, H. E., Jr., and Bragg, M. B., " Effect of Intercycle Ice Accretions on Airfoil Performance," *Proceedings of the 40th AIAA Aerospace Sciences Meetings and Exhibit*, AIAA Publishing, Reston, VA, Jan. 2002, pp. 237–245.

[9] Reinmann, J. J., Shaw, R. J., and Ranaudo, R. J., "NASA's Program on Icing Research and Technology," *Proceedings of the Symposium on Flight in Adverse Environmental Conditions*, Kluwer Publishers, Norwell, MA, May 1989, pp. 73–78.

[10] Martin, C. A., and Putt, J. C., "Advanced Pneumatic Impulse Ice Protection System (PIIP) for Aircraft," *Journal of Aircraft*, Vol. 29, No. 4, 1992, pp. 714–716.

[11] Ingram, R. B., and Gerardi, J. J., U.S. Patent Application for a "Shape Memory Alloy De-Icing Technology," Docket No. 5,686,003, filed 1997.

[12] Ramanathan, S., Varadhan, V. V., and Varadhan, V. K., "De-Icing of Helicopter Blades Using Piezoelectric Actuators," *Smart Structures and Materials 2000: Smart Electronics and MEMS*, SPIE Publishing, Seattle, WA, March 2002, pp. 354–363.

[13] Venna, S., and Lin, Y. J., "In-Flight De-Icing Self-Actuating Wing Structures with Piezoelectric Actuators," *Proceedings of American Society of Mechanical Engineers/International Mechanical Engineering Congress and Exposition 2002*, ASME Press, New York, NY, Nov. 2002, pp. 237–245.

[14] Venna, S., and Lin, Y. J., "Viable Development of Self-Actuating In-Flight De-Icing Structures with Power Consumption Considerations," *Proceedings of the American Society of Mechanical Engineers/ International Mechanical Engineering Congress and Exposition 2003*, ASME Press, New York, NY, Nov. 2003, pp. 45–53.

[15] Venna, S., and Lin, Y. J., "Mechatronic Development of Self-Actuating In-Flight De-Icing Structures," *IEEE/ASME Transactions on Mechatronics* (to be published).

[16] Raraty, L. E., and Tabor, D., "The Adhesion and Strength Properties of Ice," *Proceedings of the Royal Society of London A*, Vol. 245, No. 1, 1958, pp. 184–201.

[17] Jellinek, H. H. G., "Adhesive Properties of Ice," U.S. Army, Corps of Engineers, Research Rept. UDN1920, Vol. 38, 1957.

[18] Scavuzzo, R. J., and Chu, M. L., "Structural Properties of Impact Ices Accreted on Aircraft Structures," NASA CR-179580, 1987.

[19] Scavuzzo, R. J., Chu, M. L., and Kellackey, C. J., "Impact Ice Stresses in Rotating Airfoils," *Journal of Aircraft*, Vol. 28, No. 7, 1991, pp. 450–455.

[20] Bascom, W. D., Cottington, R. L., and Singleterry, C. R., "Ice Adhesion to Hydrophilic and Hydrophobic Surfaces," *The Journal of Adhesion*, Vol. 1, No. 2, 1969, pp. 246–263.

[21] Archer, P., and Gupta, V., "Measurement and Control of Ice Adhesion to Aluminium 6061 Alloy," *Journal of the Mechanics and Physics of Solids*, Vol. 46, No. 10, 1998, pp. 1745–1771.

[22] Buck, R., *Aircraft Icing Handbook*, Safety Education and Publishing Unit, Civil Aviation Authority, Lower Hutt, New Zealand, 2000, pp. 8–10.

[23] Venna, S., "Development of Self-Actuated In-Flight De-Icing Technology Utilizing Smart Structure Concepts," Ph.D. Dissertation, Department of Mechanical Engineering, University of Akron, Akron, OH, 2005.